

Modulation Doping of a Mott Quantum Well by a Proximate Polar Discontinuity

T. Higuchi,^{1,*} Y. Hotta,¹ T. Susaki,¹ A. Fujimori,² and H. Y. Hwang^{1,3}

¹*Department of Advanced Materials Science,
University of Tokyo, Kashiwa, Chiba 277-8561, Japan*

²*Department of Physics, University of Tokyo,
Bunkyo-ku, Tokyo 113-0033, Japan*

³*Japan Science and Technology Agency, Kawaguchi, 332-0012, Japan*

(Dated: April 25, 2019)

Abstract

We present evidence for hole injection into $\text{LaAlO}_3/\text{LaVO}_3/\text{LaAlO}_3$ quantum wells near a polar surface of LaAlO_3 (001). As the surface is brought in proximity to the LaVO_3 layer, an exponential drop in resistance and a decreasing positive Seebeck coefficient is observed below a characteristic coupling length of 10-15 unit cells. We attribute this behavior to a crossover from an atomic reconstruction of the AlO_2 -terminated LaAlO_3 surface to an electronic reconstruction of the vanadium valence. These results suggest a general approach to tunable hole-doping in oxide thin film heterostructures.

PACS numbers: 73.40.-c, 71.28.+d, 73.50.Lw, 71.30.+h

I. INTRODUCTION

Surfaces and interfaces of oxides have been of growing interest, partially because of the rich variety of bulk oxide functionalities¹, as well as their unique reconstruction mechanisms^{2,3,4} not found in conventional semiconductors^{5,6}. The observation of metallic interfaces between two perovskite insulators, LaAlO₃ and SrTiO₃², has motivated many studies on the origin of this conductivity. Two scenarios have been proposed, one based on electronic reconstructions driven by the polar discontinuity at the interface^{7,8,9}, and another based on growth induced oxygen vacancies^{10,11}.

The polar discontinuity scenario examines the built-in charge structure at the interface. From an ionic point of view, LaAlO₃ is polar along the (001) direction with alternate stacking of (LaO)⁺ and (AlO₂)⁻ layers, while SrTiO₃ is non-polar with (SrO)⁰ and (TiO₂)⁰ layers. When one unit cell (uc) of LaAlO₃ is placed on SrTiO₃, there is a dipole shift in the electrostatic potential. Additional LaAlO₃ layers build up this dipole shift, leading to a diverging potential in the limit of infinite LaAlO₃ thickness. To prevent this catastrophic situation, injection of $-q/2$ (where q is the elementary charge) per 2D uc is needed at the (AlO₂)⁻-(LaO)⁺-(TiO₂)⁰-(SrO)⁰ interface, which can be accommodated by a partial valence change of Ti⁴⁺ to Ti³⁺ near the interface. The Ti³⁺ component provides mobile SrTiO₃ conduction electrons in this picture⁷. Alternatively, it has been proposed that the essential origin of the conducting interface is the formation of SrTiO₃ surface oxygen vacancies during the highly kinetic growth of films by pulsed laser deposition (PLD)^{10,11}. SrTiO₃ is known to be a material which easily accommodates oxygen vacancies that readily dope itinerant electrons¹². Discriminating between these two proposed scenarios has been controversial, in part because both mechanisms could give similar transport and spectroscopic signatures.

The LaAlO₃/SrTiO₃ system actually involves two polar discontinuities - the interface just described, as well as the polar AlO₂-terminated surface of LaAlO₃, which requires a net $+q/2$ per 2D uc. Recently it was found that the conducting LaAlO₃/SrTiO₃ interface exhibited a transition to an insulating state when the LaAlO₃ was thinner than a critical thickness of 4 uc, bringing the two polar discontinuities close together⁹. (Similar behavior was also observed for proximity coupling of two LaAlO₃/SrTiO₃ interface polar discontinuities with opposite sign⁸.) This critical thickness may be interpreted as the threshold dipole shift below which it is energetically favorable to remain in an unreconstructed state for both

the surface and the interface¹³. A different but equivalent perspective is that the polar AlO₂-terminated surface of LaAlO₃ is compensating the electrons at the LaAlO₃/SrTiO₃ interface by hole-doping on short length scales. Far above the critical thickness, the polar LaAlO₃ (001) surface atomically reconstructs via surface off-stoichiometry and surface relaxation; electronic reconstructions are unavailable because of the fixed valence of La, Al, and O^{14,15,16}. Below a characteristic coupling distance, however, hole-doping provides an alternative electronic reconstruction if it is energetically favorable.

In order to test this possibility of hole-doping, we have studied the transport properties of the Mott insulator LaVO₃ embedded in LaAlO₃ in trilayer structures [Fig. 1(a)]. LaVO₃ is an attractive candidate since it can be readily hole-doped by chemical substitution¹⁷, and because of its structural and thermodynamic compatibility with LaAlO₃ for the growth of atomically precise thin film structures. Although LaVO₃ has the same polar structure as LaAlO₃, and hence no polar discontinuity at their interface, we find an exponential drop in resistance when a polar AlO₂-terminated surface of LaAlO₃ is brought in close proximity to the LaVO₃ quantum well. Furthermore, the positive thermopower voltage measured indicates hole-like carriers, which scales with the doping dependence of bulk LaVO₃. These results indicate that polar discontinuities can be utilized for the tunable doping of holes, which cannot arise by growth induced oxygen vacancies.

II. METHODS

LaAlO₃ (n uc)/LaVO₃ (m uc)/LaAlO₃ (substrate) heterostructures (LAO(n)/LVO(m)) were fabricated by PLD, using a KrF excimer laser with a laser fluence of 1.0 J/cm², a spot size of 1.6 mm², and repetition rate of 8 Hz. The thickness of each layer was monitored by reflection high-energy electron diffraction (RHEED) oscillations [Fig. 1(b)]. AlO₂-terminated LaAlO₃ (001) single crystal substrates were preannealed at 950 °C for 30 minutes, and m uc ($m = 1$ to 30) LaVO₃ layers were deposited, followed by n uc ($n = 1$ to 50) LaAlO₃ capping layers using LaVO₄ polycrystalline and LaAlO₃ single crystal targets, respectively. The growth temperature was 600 °C and the oxygen partial pressure was 1.0×10^{-6} Torr for all processes. These conditions follow our previous optimization of high quality LaVO₃ thin film growth in the layer-by-layer growth mode¹⁸, with one exception. Note the different laser conditions: we now use a 4 lens afocal zoom stage to accurately image an aperture,

rather than a single lens just off of the focusing condition. This is far less sensitive to the divergence characteristics of the laser, and hence much more reproducible between systems. We confirmed that one RHEED oscillation corresponds to the formation of one perovskite unit cell by characterizing superlattices of LaAlO_3 and LaVO_3 using x-ray diffraction.

The stoichiometry of LaVO_3 films grown in these conditions has been confirmed from several different perspectives in previous studies. The film lattice volume was found to be close to bulk (accounting for the compressive strain by the substrate) – usually, in the presence of significant cation defects, there is significant lattice expansion of the lattice¹⁸. LaVO_3 films were also studied extensively by scanning transmission electron microscopy and electron energy-loss spectroscopy (EELS)¹⁹. The insulating LaVO_3 films have a clear V^{3+} valence, as observed in the $\text{V-L}_{2,3}$ edge. Any significant doping by off-stoichiometry would have shown clear deviations from V^{3+} spectra. Thus the stoichiometry of our LaVO_3 films has been well established in these previous studies. $\text{LaAlO}_3/\text{LaVO}_3/\text{LaAlO}_3$ quantum wells could not be grown at higher oxygen partial pressures than used here, due to the competing formation of polycrystalline $\text{LaV}^{5+}\text{O}_4$ ^{18,19}. Furthermore, the LaVO_3 layers in the as-grown quantum wells converted to the insulating, transparent (d^0) $\text{LaV}^{5+}\text{O}_4$ phase upon oxygen post annealing.

The film surface was investigated by atomic force microscopy (AFM), and all structures were atomically flat with a clear step and terrace structure reflecting the slight miscut angle of the substrate [Fig. 1(c)]. The step size (~ 0.4 nm) was consistent with the height of one LaAlO_3 uc (pseudocubic lattice constant $a_{\text{LaAlO}_3} = 0.379$ nm). Ohmic contacts were made to the buried quantum well layers using indium ultrasonic soldering, which penetrated more than 40 nm from the surface as confirmed using buried SrVO_3 test structures.

III. RESULTS AND DISCUSSION

A. LaAlO_3 cap thickness dependence

The in-plane sheet resistance was dramatically dependent on the LaAlO_3 cap thickness as shown in Fig. 2(a), where the thickness of the LaVO_3 layer was fixed to 3 uc. Below a characteristic thickness of around 10-15 uc, the sheet resistance decreased exponentially. For all samples the sheet resistance showed Arrhenius-type thermally activated behavior as

shown in the inset of Fig. 2(b). The activation energy was ~ 0.7 eV for the thick capping layer samples, and decreased to ~ 0.1 eV with a similar characteristic thickness. Since LaAlO_3 is such a robust insulator (both in bulk and as measured in our thin films), the resistance of the embedded LaVO_3 layer could be measured to the very high values shown.

Similar results were found for these $\text{LAO}(n)/\text{LVO}(3)$ trilayer structures further capped with a non-polar material, 10 uc of SrTiO_3 , but measurement was limited to a lower range of resistance values ($n \leq 8$) by the higher intrinsic conductivity of SrTiO_3 . This suggests that the conductivity of the LaVO_3 layer only depends on the distance to the polar surface (LaAlO_3 surface) or interface ($\text{SrTiO}_3/\text{LaAlO}_3$), not on the total thickness of the material deposited on top of it. Therefore, the role of LaVO_3 defects created during growth of the cap can be neglected here.

These results are well explained by the electrostatic coupling of reconstructions of the polar surface and the quantum well, as illustrated in Fig. 3. Since we fabricated the quantum well structures by perovskite unit cell deposition on AlO_2 -terminated LaAlO_3 substrates, the surface of the LaAlO_3 cap preserves AlO_2 -termination, which requires a net $+q/2$ per 2D uc to avoid the potential divergence arising from the surface polar discontinuity. Here we consider two reconstruction mechanisms for this system. The first possibility is hole injection into the LaVO_3 quantum well layer. In this case we have no divergence, but still a finite dipole shift $\Delta(n)$ arising from the polar LaAlO_3 cap. Thus the total energy of this electronic reconstruction is the sum of the energy cost to change the vanadium valence E_{val} and $\Delta(n)$. The second process is the normal surface reconstruction of LaAlO_3 where an atomic reconstruction is dominant (oxygen vacancies and lattice distortions) to provide positive charge. This reconstruction requires an energy cost E_{sur} which is nominally independent of the thickness of the cap layer. Note that this is the same E_{sur} , calculated in Ref. [20] with respect to E_{val} for Ti, where the conducting $\text{LaAlO}_3/\text{SrTiO}_3$ interface is toggled by manipulating the surface reconstruction. The difference in E_{val} for Ti and V leads to the different critical thickness observed in the two systems.

In the simplest form, $\Delta(n)$ increases linearly as a function of the LaAlO_3 cap thickness: $\Delta(n) = nq/2\varepsilon a_{\text{LaAlO}_3}$ (ε is the dielectric constant of LaAlO_3). If the cap is sufficiently thin (and $E_{val} < E_{sur}$), then $E_{val} + \Delta(n) < E_{sur}$ and hole injection is dominant, which decreases the resistance of the quantum well. On the other hand, when the cap is very thick, $E_{val} + \Delta(n) > E_{sur}$, and the surface of the LaAlO_3 cap is reconstructed, while the

LaVO₃ layers are undoped and insulating. Between these limiting cases, hole injection into the LaVO₃ layer gradually decreases and the resistance increases as a function of the cap thickness, as observed in the transport measurements. Taking the LaAlO₃ bulk dielectric constant $\varepsilon = 24\varepsilon_0$ (ε_0 is the vacuum permittivity), $\Delta(10) = 9.9$ eV, exceeding the LaAlO₃ bulk bandgap ~ 5.6 eV. In the actual system this is greatly reduced by strong polarization of the LaAlO₃ lattice as observed by surface x-ray diffraction in LaAlO₃ thin films on SrTiO₃²¹. Thus the detailed response is far more complex than represented in Fig. 3, and the energy cost $\Delta(n)$ is likely dominated by the polarization energy of LaAlO₃. A further discussion of the contrast in LaAlO₃ thickness dependence of the conductivity observed here (conductivity in the thin limit), with prior results for the (001)-oriented LaAlO₃/SrTiO₃ and LaVO₃/SrTiO₃ interfaces^{9,22} (conductivity in the thick limit), is given in the Appendix.

Note that Fig. 3 only shows the near surface region with the LaVO₃ quantum well. To formally confirm that global charge neutrality is maintained for the total system in all cases of reconstructions, the structure of the bottom surface must be known. This can best be illustrated in the schematic shown in Fig. 4, where we discuss only polar surfaces of LaAlO₃ for simplicity.

As is well established in surface science, the polar surfaces are unstable to reconstructions driven to keep the electrostatic potential bounded. For case A, each surface requires $+e/2$ charge to achieve this. This net $+e$ is compensated by the extra $(\text{AlO}_2)^-$ layer in the total structure, thus preserving global charge neutrality. For case B, the top surface requires $+e/2$ charge, the bottom surface $-e/2$ charge, and since the number of $(\text{AlO}_2)^-$ layers and $(\text{LaO})^+$ layers are equal, here again global charge neutrality is conserved. Note that in case B, one could say that the $e/2$ was transferred from the bottom to the top surface, while in case A, $e/2$ may be considered to arise locally. In either case, the reconstruction of the top $(\text{AlO}_2)^-$ surface is identical, although to formally conserve total charge, knowledge of the bottom interface is needed. Practically, these two surfaces are completely decoupled (the thickness of our substrates are 0.5 mm, and certainly changing the termination layer on one surface does not affect the other across this macroscopic distance), so we address only the top surface in Fig. 3, as is conventional in such discussions of polar surfaces. Therefore our conclusions are independent of the assignment of charge transfer. Only when polar surfaces are microscopically close^{8,9,22} do they couple.

B. Thermoelectric power

A critical test of this model of coupled surface and interface reconstructions would be whether the carriers induced by the electronic reconstruction are holes, not electrons as in all previous examples^{2,7,8,9,10,11}. They should further be tunable with the LaAlO₃ cap layer thickness. To determine the sign of the transport carriers, the Seebeck coefficient S of the LAO(n)/LVO(3) structures was measured, as shown in Fig. 5. Intrinsic voltage fluctuations at high impedance limited the measurements to higher temperatures and thin LaAlO₃ cap samples. The positive sign of S confirms hole-doping, and it systematically increased as a function of increasing LaAlO₃ capping layer thickness, indicating a decreasing hole density and mirroring the evolution of the sheet resistance shown in Fig. 2. These results agree well with thermopower measurements of bulk La_{1-x}Sr_xVO₃ and La_{1-x}Ca_xVO₃, where S was positive for $0 < x < 0.2$ and decreased as the dopant concentration x increased^{23,24,25,26}. Given the compressive strain arising from the LaAlO₃ substrate, the reduced electronic bandwidth, and interface scattering, a comparison between these LaVO₃ quantum wells and bulk values is an approximate one. Nevertheless, this comparison indicates that the maximum equivalent hole density achieved in the single uc LaAlO₃ cap sample is just below the bulk metal-insulator transition, occurring at $x = 0.18$ in La_{1-x}Sr_xVO₃¹⁷. A recent theoretical proposal suggests that doped holes at LaVO₃ interfaces are susceptible to charge ordering due to the artificial confined geometry²⁷, which may be relevant here.

C. LaVO₃ thickness dependence

In the regime of a thin LaAlO₃ cap layer, a V⁴⁺ component giving rise to these holes should be observable. This has indeed been seen recently by x-ray photoemission spectroscopy on LAO(3)/LVO(m) structures (grown on SrTiO₃ substrates)²⁸. In particular, the spatial distribution was highly asymmetric, with the V⁴⁺ predominantly in the topmost LaVO₃ layer. This non-uniformity naturally arises in Fig. 3(b), since $\Delta(n)$ would thus be minimized. The detailed charge distribution is a balance between $\Delta(n)$ and the electronic compressibility. This issue was further studied by measuring the transport properties of LAO(3)/LVO(m) quantum well structures. As shown in Fig. 6, the sheet resistance was strongly dependent on the LaVO₃ layer thickness m . The data did not scale with $1/m$, as would be expected

for a uniform 3D resistivity. For $m > 10$, there was little change in the sheet resistance, but for $m < 6$ it increased more rapidly than $1/m$, indicating the length scale for strong perturbation of the charge distribution by confinement effects. Thus the thickness dependent resistance indicates that the conducting holes were distributed primarily at the top of the LaVO_3 layer, as would be expected for doping arising from the polar LaAlO_3 surface.

IV. SUMMARY

We have found a strong electrostatic coupling between the AlO_2 -terminated LaAlO_3 (001) surface and an embedded LaVO_3 quantum well. When they are separated by less than 4-6 nm, transport measurements indicate systematically increasing hole-doping with decreasing separation. We propose that these results reflect a competition between atomic and electronic reconstructions, driven by the need to resolve the divergent surface energy arising from the polar surface termination. An important aspect of this study is that the electronic reconstruction involves holes, not electrons. Therefore the role of polar discontinuities can be more clearly distinguished from that of electron-donor oxygen vacancies, in contrast to previous examples. They further demonstrate that oxide heterostructures can be designed to introduce carriers without local chemical substitution, in analogy to modulation doping in compound semiconductor heterostructures.

Acknowledgments

We thank Y. Hikita, K. Itaka, and T. Higuchi (Sr.) for helpful discussions. We acknowledge support from a Grant-in-Aid for Scientific Research on Priority Areas. Y. H. acknowledges partial support from QPEC, Graduate School of Engineering, University of Tokyo.

Appendix

Comparison of LaAlO_3 Thickness-Dependent Conductivity in $\text{LaAlO}_3/\text{LaVO}_3/\text{LaAlO}_3$ (001) with $\text{LaAlO}_3/\text{SrTiO}_3$ (001) and $\text{LaVO}_3/\text{SrTiO}_3$ (001)

It is worth contrasting the LaAlO_3 thickness dependence for the interface hole-doping we find here, with prior results for electron-doping at the (001)-oriented $\text{LaAlO}_3/\text{SrTiO}_3$ interface⁹ (and (001)-oriented $\text{LaVO}_3/\text{SrTiO}_3$ interface²²). For the $\text{LaAlO}_3/\text{SrTiO}_3$ structures, there are two polar discontinuities, the LaAlO_3 surface and the $\text{LaAlO}_3/\text{SrTiO}_3$ interface. Without any reconstruction, the finite shift Δ remains, as shown in Fig. 7(a). When the LaAlO_3 layer is thick, the large Δ makes the system unstable, and the polar discontinuities are reconstructed in order to solve the instability – the LaAlO_3 surface as shown in Fig. 7(b), and the $\text{LaAlO}_3/\text{SrTiO}_3$ interface by inducing Ti valence changes and associated metallic behavior as shown in Fig. 7(c). However, one reconstruction just by the LaAlO_3 surface or by the $\text{LaAlO}_3/\text{SrTiO}_3$ interface alone is insufficient and the electrostatic potential diverges. Therefore, when the two polar discontinuities are far apart from each other and the potential shift Δ in Fig. 7(a) becomes large, both must reconstruct simultaneously, as shown in Fig. 7(d). Only when they are brought close together can they couple and remain unreconstructed^{8,9,22}. Thus the $\text{LaAlO}_3/\text{SrTiO}_3$ interface is insulating for thin LaAlO_3 layers [Fig. 7(a)], and metallic in the thick limit [Fig. 7(d)].

For the $\text{LaAlO}_3/\text{LaVO}_3/\text{LaAlO}_3$ structures, there is only one polar discontinuity, the polar LaAlO_3 surface. For a LaVO_3 layer embedded in LaAlO_3 far from any surface, there are no discontinuities to resolve, and thus no reconstructions induced. Only when the LaVO_3 layer is brought in proximity to the polar LaAlO_3 surface does it provide an alternative reconstruction mechanism, by V valence changes. Therefore conductivity appears only in the thin limit, opposite to that for the $\text{LaAlO}_3/\text{SrTiO}_3$ interface.

* E-mail: higuchi@hwang.k.u-tokyo.ac.jp

¹ M. Imada, A. Fujimori, and Y. Tokura, Rev. Mod. Phys. **70**, 1039 (1998).

² A. Ohtomo and H. Y. Hwang, Nature (London) **427**, 423 (2004).

- ³ S. Okamoto and A. J. Millis, *Nature (London)* **428**, 630 (2004).
- ⁴ W.-C. Lee and A. H. MacDonald, *Phys. Rev. B* **74**, 075106 (2006).
- ⁵ G. A. Baraff, J. A. Appelbaum, and D. R. Hamann, *Phys. Rev. Lett.* **38**, 237 (1977).
- ⁶ W. A. Harrison, E. A. Kraut, J. R. Waldrop, and R. W. Grant, *Phys. Rev. B* **18**, 4402 (1978).
- ⁷ N. Nakagawa, H. Y. Hwang, and D. A. Muller, *Nat. Mater.* **5**, 204 (2006).
- ⁸ M. Huijben, G. Rijnders, D. H. A. Blank, S. Bals, S. V. Aert, J. Verbeeck, G. V. Tendeloo, A. Brinkman, and H. Hilgenkamp, *Nat. Mater.* **5**, 556 (2006).
- ⁹ S. Thiel, G. Hammerl, A. Schmehl, C. W. Schneider, and J. Mannhart, *Science* **29**, 313 (2006).
- ¹⁰ A. Kalabukhov, R. Gunnarsson, J. Borjesson, E. Olsson, T. Claeson, and D. Winkler, *Phys. Rev. B* **75**, 121404(R) (2007).
- ¹¹ W. Siemons, G. Koster, H. Yamamoto, W. A. Harrison, G. Lucovsky, T. H. Geballe, D. H. A. Blank, and M. R. Beasley, *Phys. Rev. Lett.* **98**, 196802 (2007).
- ¹² See D. A. Muller, N. Nakagawa, A. Ohtomo, J. L. Grazul, and H. Y. Hwang, *Nature (London)* **430**, 657 (2004), and references therein.
- ¹³ H. Y. Hwang, *Science* **313**, 1895 (2006).
- ¹⁴ J. Yao, P. B. Merrill, S. S. Perry, D. Marton, and J. W. Rabalais, *J. Chem. Phys.* **108**, 1645 (1998).
- ¹⁵ R. J. Francis, S. C. Moss, and A. J. Jacobson, *Phys. Rev. B* **64**, 235425 (2001).
- ¹⁶ C. H. Lanier, J. M. Rondinelli, B. Deng, R. Kilaas, K. R. Poeppelmeier, and L. D. Marks, *Phys. Rev. Lett.* **98**, 086102 (2007).
- ¹⁷ S. Miyasaka, T. Okuda, and Y. Tokura, *Phys. Rev. Lett.* **85**, 5388 (2000).
- ¹⁸ Y. Hotta, Y. Mukunoki, T. Susaki, H. Y. Hwang, L. Fitting, and D. A. Muller, *Appl. Phys. Lett.* **89**, 031918 (2006).
- ¹⁹ L. F. Kourkoutis, Y. Hotta, T. Susaki, H. Y. Hwang, and D. A. Muller, *Phys. Rev. Lett.* **97**, 256803 (2006).
- ²⁰ C. Cen, S. Thiel, G. Hammerl, C. W. Schneider, K. E. Andersen, C. S. Hellberg, J. Mannhart, and J. Levy, *Nat. Mater.* **7**, 298 (2008).
- ²¹ V. Vonk, M. Huijben, K. J. I. Driessen, P. Tinnemans, A. Brinkman, S. Harkema, and H. Graaf-sma, *Phys. Rev. B* **75**, 235417 (2007).
- ²² Y. Hotta, T. Susaki, and H. Y. Hwang, *Phys. Rev. Lett.* **99**, 236805 (2007).
- ²³ M. Sayer, R. Chen, R. Fletcher, and A. Mansingh, *J. Phys. C* **8**, 2059 (1975).

- ²⁴ J. B. Webb and M. Sayer, *J. Phys. C* **9**, 4151 (1976).
- ²⁵ P. Dougier and P. Hagenmuller, *J. Solid State Chem.* **15**, 158 (1975).
- ²⁶ H. C. Nguyen and J. B. Goodenough, *Phys. Rev. B* **52**, 8776 (1995).
- ²⁷ G. Jackeli and G. Khaliullin, *cond-mat/0904.3974*.
- ²⁸ Y. Hotta, H. Wadati, A. Fujimori, T. Susaki, and H. Y. Hwang, *Appl. Phys. Lett.* **89**, 251916 (2006).

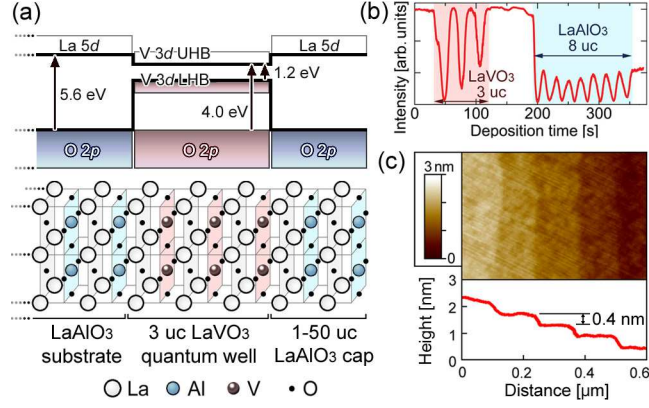


FIG. 1: (Color online) (a) Schematic band diagram and crystal structure of LAO(*n*)/LVO(3) quantum wells grown on AlO₂-terminated LaAlO₃ (001) substrates. Filled and empty bands correspond to the valence and conduction bands, respectively, and O 2*p* bands are assumed to be aligned. (b) Typical RHEED oscillations during growth of LAO(8)/LVO(3). (c) AFM image of LAO(50)/LVO(3) showing a clear step and terrace surface with step height of ~ 0.4 nm.

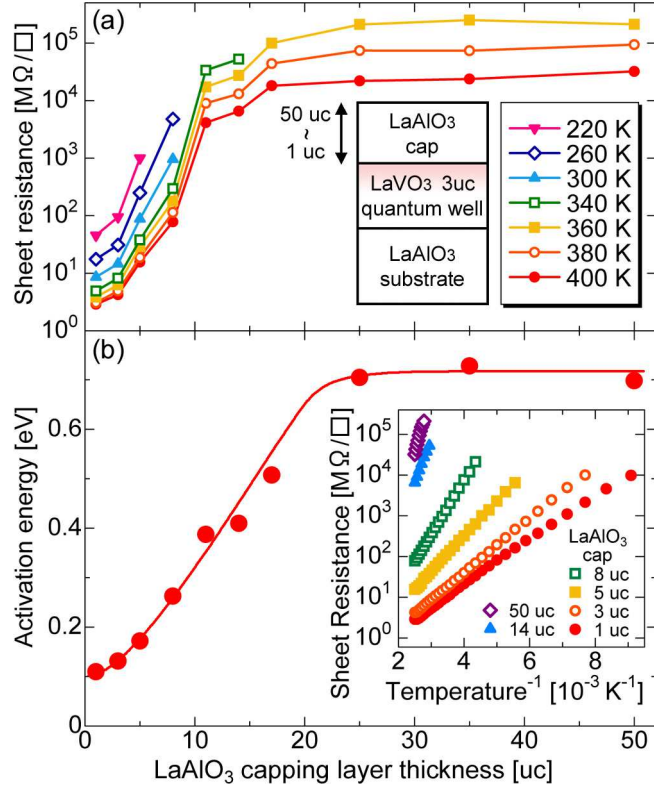


FIG. 2: (Color online) (a) Sheet resistance and (b) activation energy of LAO(n)/LVO(3) as a function of LaAlO₃ cap thickness n . The curve is a guide to the eye. Inset of (b) shows Arrhenius plots of the sheet resistance.

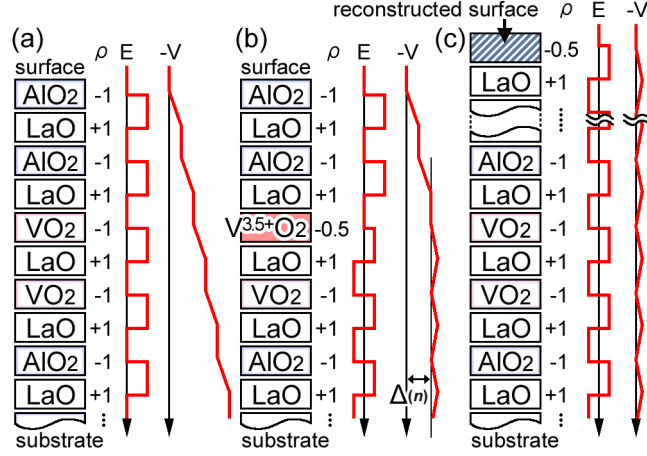


FIG. 3: (Color online) Schematic diagrams of possible reconstruction processes. (a) Without reconstruction the structure is composed of negatively and positively charged (ρ) layers from the surface, which induces a non-negative electric field (E), leading to a divergence in potential ($-V$). (b) Electronic reconstruction at the LaVO_3 quantum well layer with a net half hole per 2D unit cell induced. The potential divergence is canceled, but a finite shift $\Delta(n)$ in potential remains. (c) Atomic reconstruction of the LaAlO_3 polar surface.

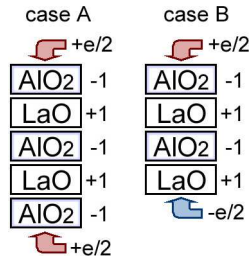


FIG. 4: (Color online) Schematic reconstructions of the top and bottom polar surfaces of (001)-oriented LaAlO_3 for two different terminations of the bottom surface.

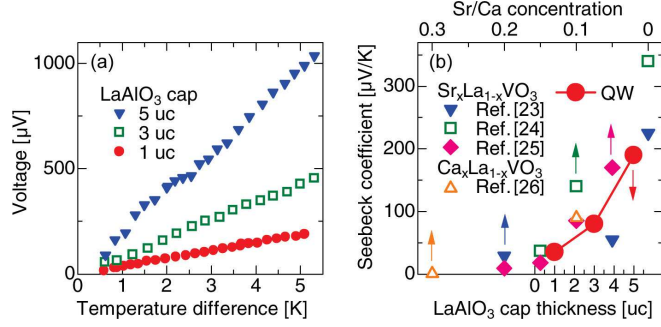


FIG. 5: (Color online) (a) Thermoelectric voltage measured as a function of applied temperature difference between two electrodes on $\text{LAO}(n)/\text{LVO}(3)$ quantum wells at room temperature. (b) Seebeck coefficient of $\text{LAO}(n)/\text{LVO}(3)$ as a function of n (filled circles), plotted in comparison with bulk values for $\text{La}_{1-x}\text{Sr}_x\text{VO}_3$ (Refs. [23,24,25]) and $\text{La}_{1-x}\text{Ca}_x\text{VO}_3$ (Ref. [26]) at 300 K.

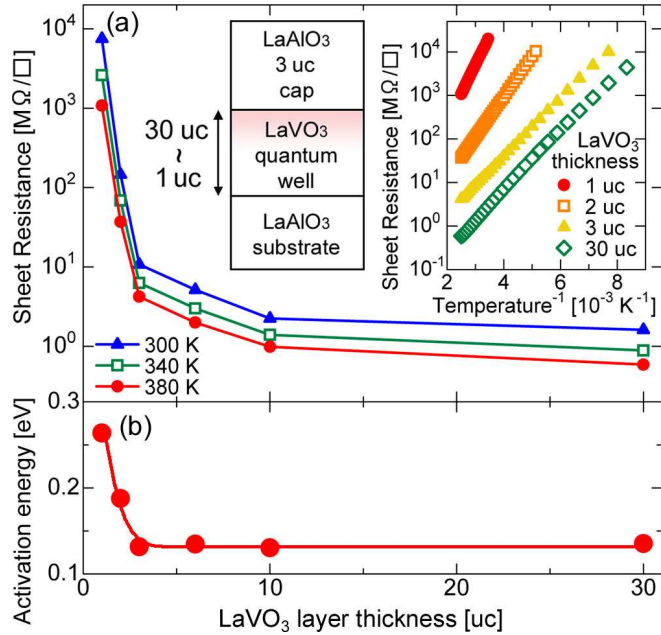


FIG. 6: (Color online) (a) Sheet resistance and (b) activation energy of $\text{LAO}(3)/\text{LVO}(m)$ as functions of LaVO_3 layer thickness m . Inset of (a) shows Arrhenius plots of the sheet resistance. The curve is a guide to the eye.

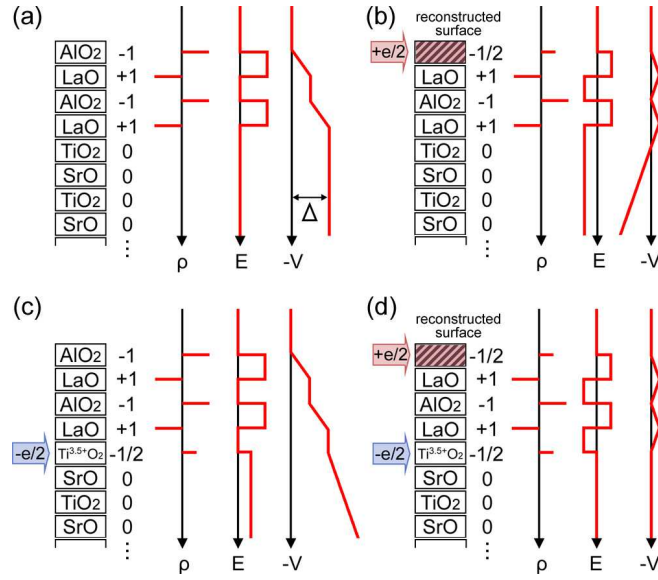


FIG. 7: (Color online) Schematic reconstructions of the polar surface of (001)-oriented LaAlO₃ and the LaAlO₃/SrTiO₃ interface. (a) No reconstruction, (b) only the LaAlO₃ surface is reconstructed, (c) only the LaAlO₃/SrTiO₃ interface is reconstructed, and (d) both are reconstructed.